

A. Jaros, S. Bley, K. Zimmermann, L. Krieg, A. Castro-Carranza, J. Gutowski, F. Meierhofer, T. Voss

Optical Properties and Carrier Dynamics in Inorganic and Hybrid Inorganic/Organic ZnO- and GaN-based Nanowire Structures Feature Article FOR1616

Journal Article as: peer-reviewed accepted version (Postprint)

DOI of this document* (secondary publication): <https://doi.org/10.26092/elib/3692>

Publication date of this document: 17/02/2025

* for better findability or for reliable citation

Recommended Citation (primary publication/Version of Record) incl. DOI:

Jaros, A., Bley, S., Zimmermann, K., Krieg, L., Castro-Carranza, A., Gutowski, J., Meierhofer, F. and Voss, T. (2019), Optical Properties and Carrier Dynamics in Inorganic and Hybrid Inorganic/Organic ZnO- and GaN-Based Nanowire Structures. *Phys. Status Solidi B*, 256: 1800463. <https://doi.org/10.1002/pssb.201800463>

Please note that the version of this document may differ from the final published version (Version of Record/primary publication) in terms of copy-editing, pagination, publication date and DOI. Please cite the version that you actually used. Before citing, you are also advised to check the publisher's website for any subsequent corrections or retractions (see also <https://retractionwatch.com/>).

This is the peer reviewed version of the article cited above, which has been published in final form at <https://doi.org/10.1002/pssb.201800463>. This article may be used for non-commercial purposes in accordance with Wiley Terms and Conditions for Use of Self-Archived Versions. This article may not be enhanced, enriched or otherwise transformed into a derivative work, without express permission from Wiley or by statutory rights under applicable legislation. Copyright notices must not be removed, obscured or modified. The article must be linked to Wiley's version of record on Wiley Online Library and any embedding, framing or otherwise making available the article or pages thereof by third parties from platforms, services and websites other than Wiley Online Library must be prohibited.

This document is made available with all rights reserved.

Take down policy

If you believe that this document or any material on this site infringes copyright, please contact publizieren@suub.uni-bremen.de with full details and we will remove access to the material.

Optical Properties and Carrier Dynamics in Inorganic and Hybrid Inorganic/Organic ZnO- and GaN-Based Nanowire Structures

Angelina Jaros, Stephanie Bley, Kseniia Zimmermann, Linus Krieg, Alejandra Castro-Carranza, Jürgen Gutowski, Florian Meierhofer, and Tobias Voss*

In this paper, results on the optical properties and carrier dynamics in inorganic and hybrid inorganic/organic semiconductor nanowire structures based on the ZnO and GaN material systems, obtained by the involved groups in the last years, are reviewed. First, the recombination dynamics in 3D GaN-based microrod LED structures is analyzed and discussed. In particular, the dynamics at high excitation densities close to the damage threshold of the material is studied. This is followed by a discussion of the carrier dynamics in nanowire structures functionalized with colloidal CdSe quantum dots (QDs) or carbon nanoparticles (C-Dots). Here, the nanoparticles allow for light absorption at photon energies below the bandgap of the semiconductor nanowire, and subsequent electron tunneling couples the electronic systems of the nanoparticles and the nanowires (NWs). Finally, the fabrication of nanowire/polymer core-shell structures is demonstrated and the electrical properties of n-nanowire/p-polymer hybrid junctions are studied.

semiconductor technologies include the small footprint of the NWs on the substrate that allows for their epitaxial growth on a large variety of different substrates.^[3,4] In addition, a high degree of integration can be achieved because a huge number of NW devices can be integrated onto a specific substrate area. Finally, the large surface-to-volume ratio of NWs makes them attractive candidates for the fabrication of hybrid inorganic/organic devices where organic materials such as linker molecules or polymer layers can be attached to the surface of NWs thus showing a strong impact on the electronic and optoelectronic properties of the hybrid nanowire structure.^[5,6]

The design of complex and often hybrid nanowire devices for optoelectronics and sensing requires a detailed knowledge of the electronic states and the dynamics of electron hole pairs excited in the wires.

1. Introduction

During the past two decades, semiconductor nanowires (NWs) have been at the focus of intense research. NW-based lasers, light-emitting diodes (LEDs), photodetectors, solar cells, and sensors are most actively studied optoelectronic devices.^[1,2] Advantages of NWs as compared to conventional planar


This information can be obtained from time-resolved optical spectroscopy performed on individual nanowire structures. Time- and spectrally resolved signals, for example, luminescence intensity or photocurrent, will yield important information about the electronic processes such as the lifetime of excited states or the impact of photo-induced chemical reaction at the NW surface or at the hybrid inorganic/organic interface.

In this paper, the optical properties and the dynamics of photo-excited charge carriers in inorganic and hybrid inorganic/organic semiconductor nanowire structures based on the ZnO and GaN material systems are discussed. ZnO and GaN are both direct wide-gap semiconductors that are transparent throughout the visible spectral region but strongly absorb in the UV.^[7-9] Whereas ZnO NWs are particularly well suited for the analysis of excitonic processes in NWs and constitute a versatile and cheap platform for NW-based sensing devices, GaN together with its alloys InGaN and AlGaN is the most important material for blue-UV or white-light-emitting NW diodes. The two material systems share the wurtzite crystal structure under typical growth conditions. However, the mainly applied growth techniques for NW structures made from these compounds strongly differ. Whereas molecular beam epitaxy (MBE)^[10] or metal-organic vapor-phase epitaxy (MOVPE)^[11] are by far dominating the fabrication of GaN-based nanowire structures, ZnO NWs are

A. Jaros, K. Zimmermann, L. Krieg, F. Meierhofer, Prof. T. Voss
Institute of Semiconductor Technology and Laboratory for Emerging
Nanometrology
Braunschweig University of Technology
Hans-Sommer-Strasse 66, 38106 Braunschweig, Germany
E-mail: tobias.voss@tu-braunschweig.de

Dr. S. Bley, Dr. A. Castro-Carranza, Prof. J. Gutowski
Institute of Solid State Physics
University of Bremen
Otto-Hahn-Allee 1, 28359 Bremen, Germany

Prof. J. Gutowski
MAPEX Center for Materials and Processes
University of Bremen
Am Fallturm 1, 28359 Bremen, Germany

 The ORCID identification number(s) for the author(s) of this article can be found under <https://doi.org/10.1002/pssb.201800463>.

most commonly obtained from a vapor-liquid-solid (VLS) growth,^[12] from wet-chemical synthesis techniques^[13,14] or from atomic-layer deposition (ALD)^[15]. We will present a summary of optical studies on MOVPE-grown GaN-based nano- and micro-wire LED structures with focus on the recombination dynamics of photo-excited electron hole pairs. We will furthermore describe the surface functionalization of ZnO NWs with colloidal CdSe quantum dots (QDs) and carbon nanodots (C-Dots) through organic linker molecules and the resulting modification of the photoconductivity of the nanowire device. Finally, we will discuss the conformal coating of arrays of ZnO NWs with ultrathin (<200 nm) layers of conductive polymers and the electronic properties of the hybrid interfaces.

2. Experimental Section

2.1. Nanowires

As explained above, different kinds of GaN- and ZnO-based semiconductor NWs and microrods were used for the time-resolved optical experiments. The GaN-based core-shell micro-rod LED structures were fabricated by MOVPE on GaN/sapphire substrates using selective area growth (SAG, performed in the group of Andreas Waag, TU Braunschweig). A few μm thick n-doped GaN layer was grown directly on the substrate before the SiO_x mask for the SAG was deposited. Afterwards, three-dimensional (3D) growth of n-GaN rods in the holes of the mask took place. An unintentionally doped GaN spacer layer and a fivefold InGaN/GaN multi quantum well (MQW) or a single quantum well (SQW) were wrapped around the microrod cores and grew mainly on the non-polar m-plane sidewalls. The capping layer consists of a few tens to hundreds nm of unintentionally doped or p-doped GaN.^[11,16]

ZnO NWs were grown either by

- 1) A hydrothermal method^[13,14] at 80–90 °C for 3–5 h on a ZnO seed layer (groups of Jürgen Gutowski, University of Bremen, and Tobias Voss, TU Braunschweig);
- 2) Atomic-layer-deposition (ALD) based atomic spacer lithography (ASL)^[15] on non-conductive sapphire/silicon ($\text{Al}_2\text{O}_3/\text{Si}$) substrates (group of Margit Zacharias, University of Freiburg);
- 3) VLS growth^[12] on silicon substrates with a 500 μm aluminum-doped zinc oxide (AZO) seed layer on top (group of Carsten Ronning, University of Jena).

The respective growth processes and the nanowire properties will be mentioned and discussed in the corresponding result sections.

Reference measurements were performed on polycrystalline ZnO layers grown by pulsed laser deposition (PLD) on sapphire substrates (group of Marius Grundmann, University of Leipzig).

2.2. Colloidal Quantum Dots and Carbon Dots

Different kinds of nanoparticles were used for surface functionalization of ZnO NWs. CdSe QDs capped with

3-mercaptopropionic acid (MPA, shortest molecule with 2 spacing moieties) were synthesized by an aqueous chemical method adopted from the literature.^[17] Commercially available CdSe QDs dissolved in toluene obtained from Ocean NanoTech were capped with 6-mercaptophexanoic acid (MHA, 5 spacing moieties) and 11-mercaptoundecanoic acid (MUA, 10 spacing moieties) via a ligand exchange method.^[18] In addition, commercially available CdSe QDs and CdSe/ZnS core-shell QDs capped with hydrophobic octadecylamine (ODA, longest molecule with 18 spacing moieties) were used.

C-Dots were prepared via hydrothermal pyrolysis of citric acid and ethylenediamine-encapped polyethylenimine (PEI-EC) at 180 °C using the approach reported elsewhere (synthesis performed in the group of Siegfried R. Waldvogel, University of Mainz).^[19] The obtained C-Dots were cleaned via column chromatography (silica) using 0.01 M HCl as an eluent and afterwards finished by freeze-drying. For further functionalization and optical characterization, the C-Dots were re-dispersed in deionized water (0.08 wt%). The pH-values of the C-Dot suspensions were adjusted by using concentrated HCl or NaOH.

2.3. Conformal Polymer Coating of Nanowires

Conformal coating of the NWs with conductive polymers was achieved by applying the oxidative chemical vapor deposition technique (oCVD).^[20,21] In brief, the gaseous monomers (EDOT, pyrrole) were introduced into the vacuum reaction chamber under a constant nitrogen carrier gas flow. Sublimated FeCl_3 was used as oxidant and was co-evaporated into the reaction chamber at temperatures >200 °C. The FeCl_3 induced a step-growth of the corresponding polymer at the substrate which was kept at temperatures between 70 and 90 °C for pyrrole and EDOT, respectively. At the same time, the incorporation of Cl resulted in a p-doping of the polymer chains through the creation of polaron and bi-polaron states.

2.4. Optical, Structural, and Electrical Characterization

The experimental set-ups used for optical, structural, and electrical characterization of the inorganic and hybrid inorganic/organic NWs have been described elsewhere.^[20–26]

Time-integrated photoluminescence (PL) measurements were performed under excitation with a continuous-wave (cw) HeCd laser ($\lambda = 325 \text{ nm}$). For pulsed excitation, different Titanium:Sapphire amplifiers were used (Solstice or Tsunami/Spitfire Pro, Spectra Physics, $\Delta t \approx 100 \text{ fs}$, $f = 1 \text{ kHz}$) in combination with an optical parametric amplifier (Topas Prime, Light Conversion).

Time-integrated detection of the PL was performed either with an Acton SP2300 spectrometer (Princeton Instruments) and a liquid-nitrogen cooled CCD camera or with a double monochromator (model SPEX 1401, Spex Industries Inc., resolution 0.3 meV, grid 1200 lines/mm) for high-resolution or with a fiber-coupled spectrometer (model 2048TEC, Avantes, resolution 2.4 nm). For time-resolved detection of the PL, a streak camera

(SC-10, Optronis) attached to the Acton spectrometer with a time resolution of $\Delta t \approx 30$ ps – 1 ns (depending on the scan speed) was used.

For electrical characterization, either a Keithley SourceMeter Model 2400 or a potentiostat-galvanostat (model PGSTAT302N, Metrohm Autolab) were used. The results shown in Figure 16 were obtained using an Agilent 4155C precision semiconductor parameter analyzer in combination with a Süss wafer-prober system P200 (group of Marius Grundmann, University of Leipzig).

For structural characterization, SEM images were taken in a FIB/SEM dual system Nova 200 (FEI, acceleration voltage 5 kV, FIB – focused ion beam), bright-field transmission scanning electron microscopy (TSEM) images were taken using the FIB/SEM dual system NanoLab 600i (FEI, acceleration voltage 30 kV), and EDX measurements were done using a JEOL SEM system JSM-6490 with included Si(Li)³ detector.

Structural characterization of ZnO NW array/C-Dot devices was performed using a FE-SEM (Zeiss Libra 35).

Photoconductivity measurements with tunable photon energies were performed using a Xenon lamp equipped with a 200 mm monochromator (10 nm bandwidth at each central wavelength between 390 and 600 nm). The resulting excitation intensities were $40 \mu\text{W cm}^{-2}$ in the blue and red spectral regions, and $80 \mu\text{W cm}^{-2}$ in the green spectral region.

3. Recombination Dynamics in 3D Microrod LED Structures

3D core-shell nanowire and microrod structures represent a promising approach for next-generation GaN-based LEDs because they allow for operating the devices at lower current densities and at the same time for reducing the production costs due to an increase in the light emitting area in core-shell structures.^[3,4,27,28] Additionally, the quantum-confined Stark effect (QCSE) does not influence the recombination dynamics of electron-hole pairs in 3D structures as the light-emitting InGaN quantum wells (QWs) are grown on the non-polar sidewalls of the GaN rods.^[29–31]

The operation of the 3D GaN-based LEDs at high excitation conditions (e.g., for high-power LEDs or even 3D laser structures) requires a detailed knowledge of the recombination dynamics of electron-hole pairs. We therefore studied these dynamics under excitation with amplified pulses from a femtosecond laser, which allows us to experimentally address excitation conditions even close to the damage threshold of the 3D structures.^[22,23]

First, we studied the influence of the high power laser pulses on the integrity and optical properties of our samples. In Figure 1 time-integrated PL spectra of one 3D MQW microrod sample are shown for different excitation conditions, with the emission intensity being normalized to the maximum InGaN luminescence. The black spectrum was taken under excitation by a HeCd laser, the others under excitation by the fs laser system with different excitation energy densities applied (room temperature, photon energy 3.81 eV). In all spectra, the GaN and InGaN luminescence bands are clearly visible with the maximum of the GaN peak at 3.36 eV. The InGaN luminescence peak blue-shifts

by about 70 meV when going from cw low-power excitation (black spectrum) to the highest pulse power used (red spectrum). The blue-shift is most likely caused by continuously filling the localized electronic states in the conduction band (CB) caused by Indium fluctuations and subsequent band-filling effects. At higher energy densities, more charge carriers are excited in the 3D structures, thus, recombination from higher-energy states increases leading to the observed blue shift of the InGaN luminescence peak. Most of the charge carriers will be trapped in the InGaN QWs, therefore, the GaN luminescence is less effected by the increase of the energy density and does not show a blue shift.^[23]

A change in the intensity ratio of the maximum GaN PL intensity relative to that of the InGaN PL can also be observed in Figure 1. The ratio increases with higher energy densities, and this change is irreversible for excitation densities $>0.05 \text{ J cm}^{-2}$. Additional investigations of a GaN layer sample, previously excited with the fs laser system with different energy densities, with an SEM revealed structural modification of the surface above the same excitation density of 0.05 J cm^{-2} and holes in the GaN layer for even higher densities. Based on this result a damage threshold of 0.05 J cm^{-2} for InGaN/GaN heterostructures can be inferred under the given excitation conditions.^[23]

The knowledge about the modification threshold allows us to perform all further investigations at energy densities being sufficiently low in order to avoid any permanent modification of the samples.

Figure 2 shows transients of the InGaN PL of a planar LED structure (black transient) and a 3D SQW microrod sample (red transient). While the recombination dynamics of the planar structure can be well described by a biexponential decay, the transient of the microrod structure shows a monoexponential decay characteristic. The decay time of the PL of the microrod structure (240 ± 30) ps and the fast component of the decay time of the planar LED (330 ± 30) ps are in the same order of magnitude. Additionally, the planar

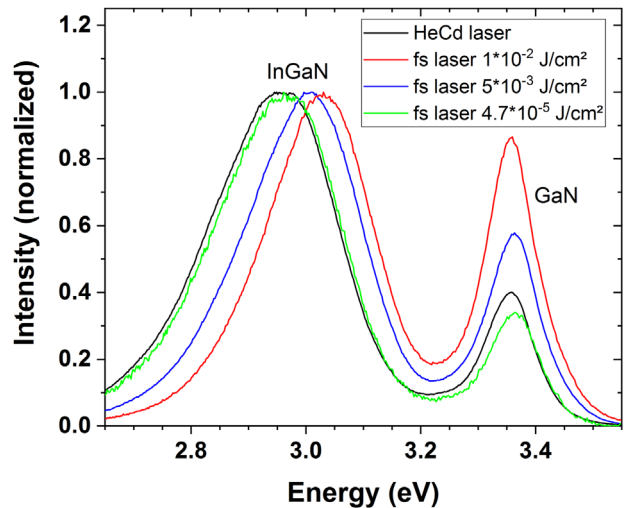


Figure 1. Normalized photoluminescence spectra of a 3D MQW microrod sample excited by a HeCd laser (black) and the fs laser system for different energy densities at 3.81 eV photon energy.

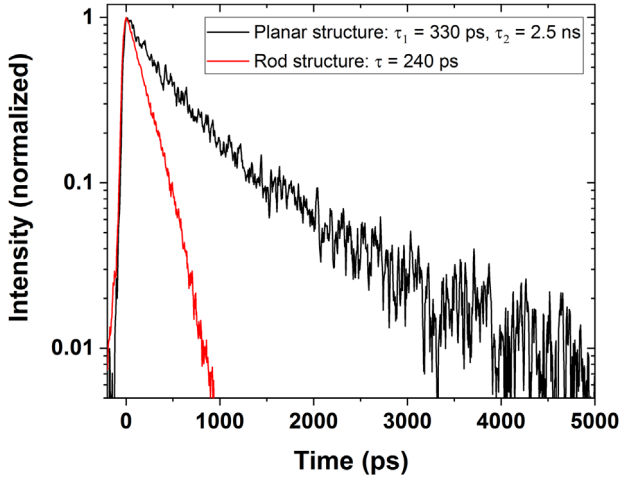


Figure 2. InGaN PL transients of a planar LED structure (black) and a SQW microrod structure (red) excited with an energy density of 0.01 J cm^{-2} and a photon energy of 3.81 eV .

structure shows a second long decay time in the range of ns which can be attributed to the QCSE. The probability of the recombination is lower because of piezoelectric fields which cause a separation of the electron and hole wave functions. The high charge carrier concentration directly after the excitation screens the QCSE and leads to the fast initial decay time.^[32] The QCSE is only present in the planar structure where the QWs are grown on the polar c-plane GaN, while for the microrods the QWs are mainly grown on the non-polar m-plane sidewalls.

We further analyzed the recombination dynamics of electron-hole pairs in the microrod structures for different temperatures, energy densities, and photon energies. In **Figure 3a** two transients of the InGaN luminescence of a SQW microrod structure are shown (energy density 0.004 J cm^{-2} , excitation photon energy 3.81 eV) at a sample temperature of 77 K (black) and 300 K (red), respectively. The decay times of

the recombination being $(210 \pm 30) \text{ ps}$ at 77 K and $(220 \pm 30) \text{ ps}$ at 300 K are nearly identical. Additionally, we performed measurements on another MQW microrod structure for several temperatures between 77 and 300 K on three different positions on the sample and two times on each position. The decay times determined from these measurements are shown in **Figure 3b** as a function of the temperature. For all three positions, the decay times increase nearly linearly with the temperature. A linear increase is reported for the radiative decay time in QWs.^[30,33–36] This leads to the assumption that in our structures non-radiative recombination plays a minor role only. The rate of the non-radiative recombination processes increases with temperature and is mainly caused by non-radiative recombination via defect states. For most structures, decreasing decay times with increasing temperature are reported because the recombination processes at higher temperatures are dominated by thermally activated electron capture in defect states.^[30,35–37] For the SQW sample the decay time is more or less stable over the investigated temperature range and shorter when compared to the one of the MQW sample at room temperature. The shorter decay time can be explained by the p-doped GaN capping layer instead of the unintentionally doped GaN layer used for the MQW sample. Due to the p-doping with Mg atoms, more defects are introduced in the sample not only in the GaN capping layer but also in the subjacent InGaN QW^[38] leading to faster recombination dynamics.

Changing the excitation conditions from non-resonant excitation (3.81 eV), that is, electron-hole pairs are generated both in the InGaN and GaN layers, to resonant conditions for the InGaN QWs (3.31 eV , no excitation in the GaN layers), we find just small changes in the PL decay characteristics for both samples (planar and 3D geometries) with slightly shorter decay times for the resonant InGaN excitation (see **Figure 4**). This can be attributed to the lack of electrons refilling the InGaN states by relaxation out of the GaN. The quite small contribution of the refilling can be explained by a fast recombination of the charge carriers in the GaN.^[39]

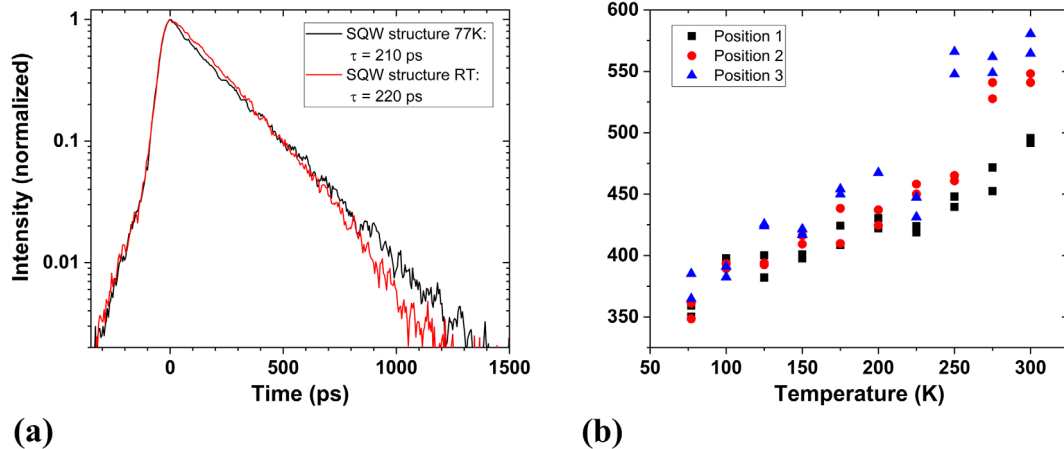


Figure 3. a) InGaN PL transients of a SQW microrod structure excited with 3.81 eV photon energy and an energy density of 0.004 J cm^{-2} at 77 K (black) and 300 K (red). b) InGaN PL decay time of a MQW microrod structure for different temperatures and three different positions on the sample. Energy density 0.05 J cm^{-2} . (b) Adapted with permission.^[22] Copyright 2017, Materials Research Society.

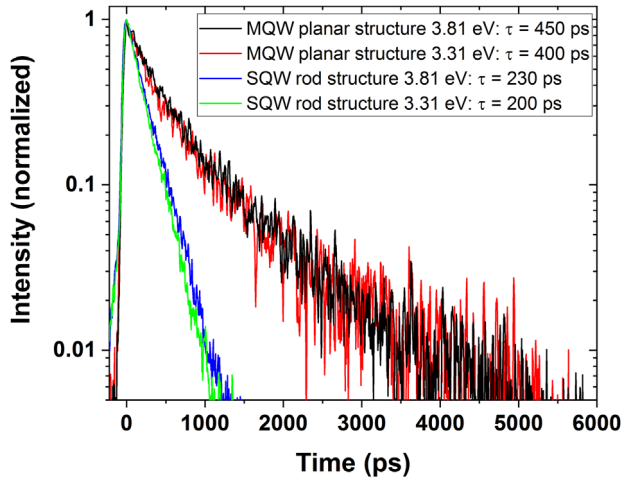


Figure 4. InGaN PL transients of a planar and a SQW microrod structure for two different excitation photon energies excited with an energy density of 0.01 J cm^{-2} for the planar and 0.004 J cm^{-2} for the SQW sample at room temperature.

Close to our determined damage threshold, we investigated the dependence of the recombination dynamics on the excitation energy density. Therefore, we used a photon energy of 3.81 eV and three different energy densities between 0.01 and 0.3 J cm^{-2} . **Figure 5** shows the transients of the InGaN luminescence of a MQW microrod sample for three different energy densities. For higher energy densities, the recombination dynamics are getting faster. The decay time reduces from (530 ± 30) ps for the lowest excitation energy density 0.01 J cm^{-2} to (320 ± 30) ps for the highest one 0.3 J cm^{-2} . At these high excitation densities, an electron-hole plasma is generated and the reduced decay time could be attributed to recombination processes in the plasma.^[40] If more charge carriers are excited, the probability for the recombination process is higher.

4. Carrier Dynamics in Hybrid CdSe QD/ZnO NW Structures

For many applications of semiconductor NWs in the field of optoelectronics, the spectral absorption and emission characteristics of the NWs have to be specifically tailored in order to match the needs of the applications. This can be achieved by the design of hybrid inorganic/organic nanowire structures, for example, colloidal semiconductor QDs attached to the nanowire surface via organic linker molecules.^[41,42] For such a hybrid system, electron transfer from the QD into the NW via tunneling processes has to be carefully studied in order to optimize the performance of the hybrid system. Time-resolved optical luminescence spectroscopy provides an easy, yet powerful tool to assess the relevant electronic states and processes, and to determine the relevant time scales.

We start with the analysis of the electron transfer from CdSe QDs and CdSe/CdS core-shell QDs which are linked to the surface of ZnO NWs (hydrothermally grown,^[13] diameter range 50–300 nm, length $\approx 2 \mu\text{m}$) with the two organic linker molecules

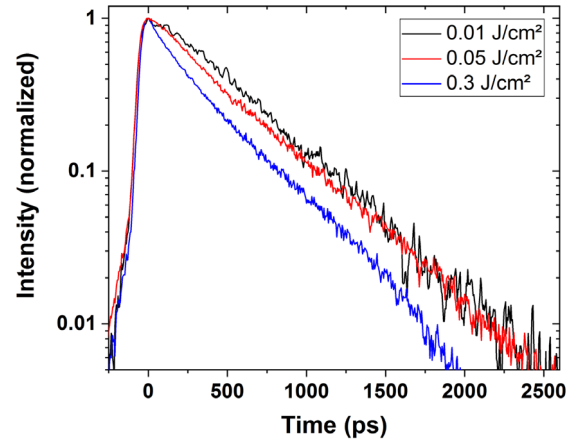


Figure 5. InGaN PL transients of a MQW microrod structure for three different excitation energy densities excited with 3.81 eV photon energy at room temperature. Adapted with permission.^[22] Copyright 2017, Materials Research Society.

octadecylamin ODA and mercaptopropionic acid MPA, respectively.^[20,24]

The PL decay of MPA-capped CdSe QDs dissolved in water, of ODA-capped CdSe QDs dissolved in toluene, and of ODA-capped CdSe/ZnS QDs dissolved in toluene and then likewise attached to ZnO NWs, respectively, are comparatively depicted in **Figure 6**. In all cases the PL decay becomes faster when the QDs are attached to the NWs and is particularly rapid during the first 10 ns after excitation. This can be explained by electron transfer from the QDs into the NWs being described by a simple rate equation model whose schematic energy diagram is shown in **Figure 7**. The model includes all relevant electron relaxation and recombination paths within the QD and the QD/NW system. Thus, the PL transients can be simulated and compared with the measurements to get information about the electron transfer times.

From the ground state 0 electrons are excited into state H. From this state, they can be trapped at surface states S within a time described by the time constant τ_{HS} . However, they can also return from S into the ground state 0 with a time constant τ_{S0} or can be thermally re-excited from S into state H with a time constant τ_{SH} . In addition, they can further relax from state H into state L with a time constant τ_{HL} , with L being the lowest excited energy state of the QD. From there, the electrons are, on the one hand, able to recombine with a time constant τ_{L0} into the ground state by emitting photons. Alternatively, on the other hand, the electrons can tunnel from state L with a time constant τ_{PET} into the CB of the ZnO NWs if the QDs are attached to the ZnO nanowire surface. All processes that eventually remove the electrons from the CB of the wires (non-radiative traps, surface states, interaction with the QD systems and the linker molecules, or recombination to the valence band [VB]) are described by the time constant τ_{ZnO} . For the details of the calculation and the used set of equations, see ref. [20].

Figure 8 shows the simulated PL transients in comparison with the measured PL transients for the QDs attached to the NWs, exhibiting an almost perfect correspondence. The calculated time constant for the photo-induced electron transfer

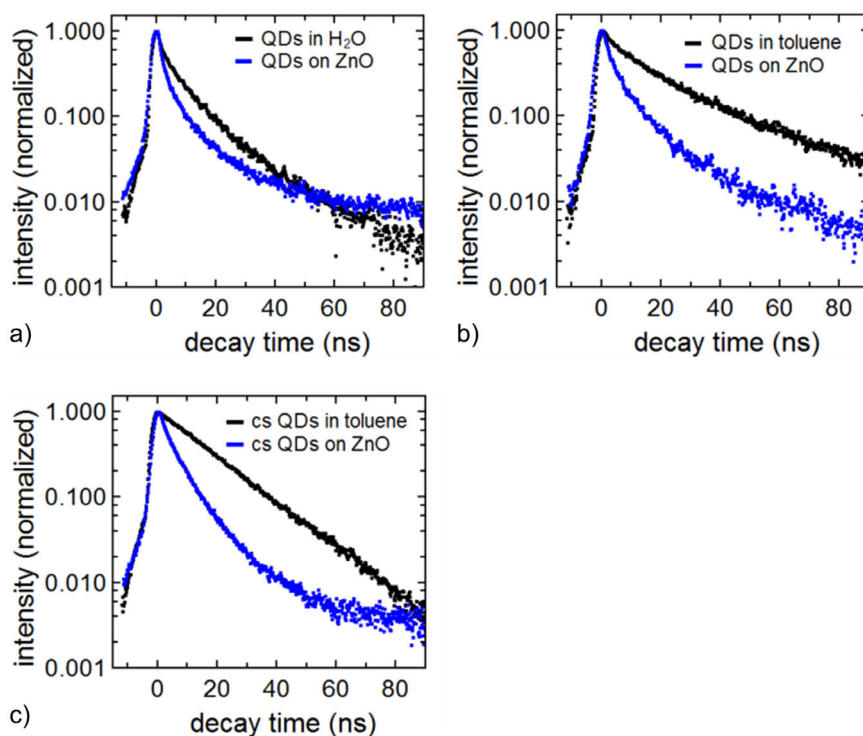


Figure 6. Normalized PL transients of (a) MPA-capped CdSe QDs in water (black) and on ZnO NWs (blue), (b) ODA-capped CdSe QDs in toluene (black) and on ZnO NWs (blue), (c) ODA-capped core-shell (cs) CdSe/ZnS QDs in toluene (black) and on ZnO NWs (blue). Adapted with permission.^[20] Copyright 2015, American Chemical Society.

τ_{PET} is given in the figures. For the calculation of τ_{PET} , it is assumed that all CdSe QDs with different linker molecules have similar optical properties so that the values for τ_{HL} , τ_{LO} , τ_{HS} , and τ_{SO} were taken as fixed mean time constants.

τ_{PET} is increasing with growing linker molecule length. In case of the core/shell QDs the shell acts like a barrier what suppresses the electron transport even more, resulting in the comparatively slowest transient.

The relatively fast photo-induced electron transport from QDs capped with short linker molecules into the ZnO NWs is

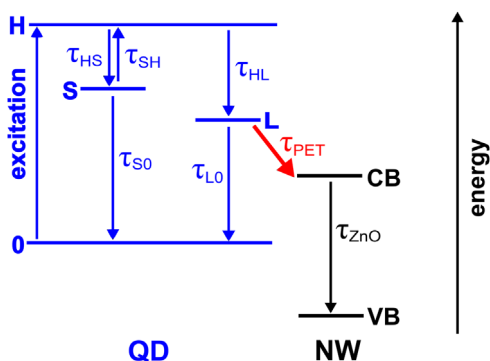


Figure 7. Schematic energy diagram: Relaxation and recombination paths inside the QD, and photo-induced electron transfer (PET) from QD to NW. Adapted with permission.^[20] Copyright 2015, American Chemical Society.

additionally confirmed by the results of photoconductivity measurements.

Figure 9 shows the photocurrent of hybrid CdSe QD/ZnO NW devices as a function of time under selective excitation of the QDs. Uncoated NWs (ALD,^[15] diameter range 300–500 nm) are compared to MPA-capped, MHA-capped, and MUA-capped QDs attached to NWs, respectively. In all cases, the dark current has been measured for ≈ 3 min before the laser light has been switched on. Since the excitation energy of the laser is below the band gap of ZnO (3.37 eV at room temperature), the uncoated NWs hardly show any significant increase of the photocurrent after switching on the laser. For the hybrid device with MPA-capped CdSe QDs the photocurrent increases quickly after laser onset and reaches saturation after 5 min, whereas, for longer linker molecule lengths, the photocurrent gets much higher but the increase becomes much slower, and saturation is not reached within a time of up to 30 min. Thus, the photocurrent dynamic slows down with increasing linker molecule length what is in good agreement with the results of the time-resolved PL measurements which have already shown that the tunneling rate decreases with increasing linker molecule length.

Oxygen molecule desorption from and readsorption on the oxide as well as from and on the QD surfaces lead to a time scale of minutes or even hours of the photocurrent changes and play an important role for the electron transfer processes between both material systems.^[43,44] The photocurrent gets saturated by reaching a dynamic equilibrium between oxygen desorption and readsorption. If linker molecules being longer than MPA are used, this equilibrium may be shifted to lower

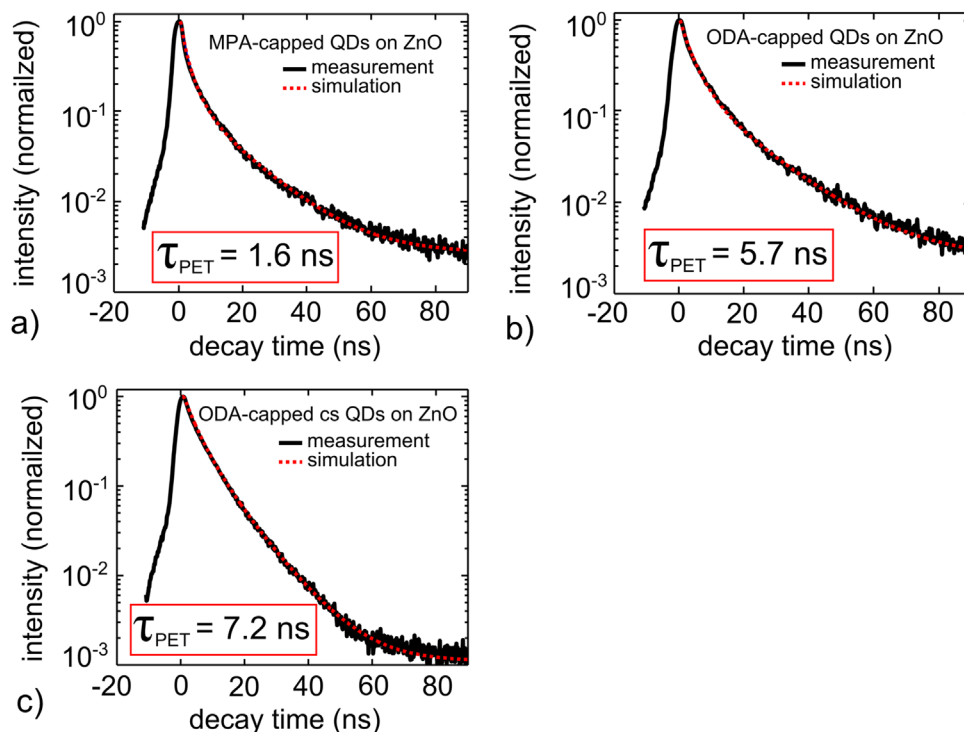


Figure 8. Normalized PL transients of the QDs attached to ZnO NWs (black curves) and corresponding simulated PL signals (red). Calculated electron transfer time constants are given in the red boxes. a) MPA-capped QDs on ZnO NWs; b) ODA-capped QDs on ZnO NWs; and c) ODA-capped core-shell QDs on ZnO NWs. Adapted with permission.^[20] Copyright 2015, American Chemical Society.

amounts of surface-adsorbed oxygen due to a diffusion barrier on the surface of the hybrid structure formed by the linker molecules. Electron diffusion through thicker barriers provided by the long linker molecules will take more time than through thinner barriers as formed by the shorter linker molecules.

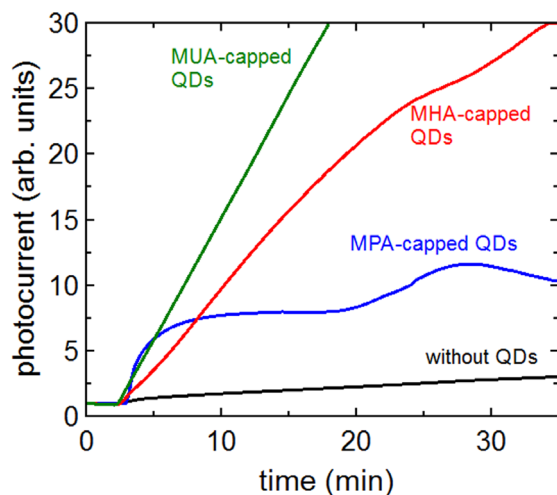


Figure 9. Photocurrent as a function of time for pure NWs and NWs coated with QDs via different linker molecules. Laser (photon energy 2.69 eV) has been switched on after ≈ 3 min measurement of dark current, respectively. Adapted with permission.^[20] Copyright 2015, American Chemical Society.

5. Carrier Dynamics in C-Dots and Sub-Band Gap Photoconductivity of ZnO NW/C-Dot Devices

CdSe QDs constitute an excellent model system for studying the surface functionalization of wide-gap semiconductor NWs and the coupling of their electronic systems. For integration into nanowire-based optoelectronic devices, however, it is mandatory to replace them with a non-toxic material which should be widely available, cheap, easy to process, and at the same time yield optically active nanoparticles with properties similar to those of CdSe-based QDs. Luminescent carbon nanoparticles, also named C-Dots, have become a widely studied class of nanomaterials during the past decade that have been shown to possess tunable optical absorption and emission bands in the visible and near-UV spectral region.^[45–48] Therefore, we have studied C-Dots in different suspensions and subsequently used these suspensions for surface functionalization of ZnO nanowire devices.^[25]

Since the functionalization of ZnO NWs requires a dispersed form of C-Dots, it is necessary to study the impact of the pH-conditions on their luminescence. The absorption and emission spectra of the studied C-Dots (at $\text{pH } 4 \pm 0.5$) can be found in our previous work.^[25]

The PL decay of C-Dot dispersions with adjusted pH-values of 3.5 and 9.5 are shown in **Figure 10**, respectively. The decay time becomes shorter as the pH-value is increased from 3.5 to 9.5. This can be explained with the charging of the surface chemical groups attached to the C-Dots. Since the studied C-Dots were prepared from an amine-containing polymer (PEI-EC) and carboxylic acid

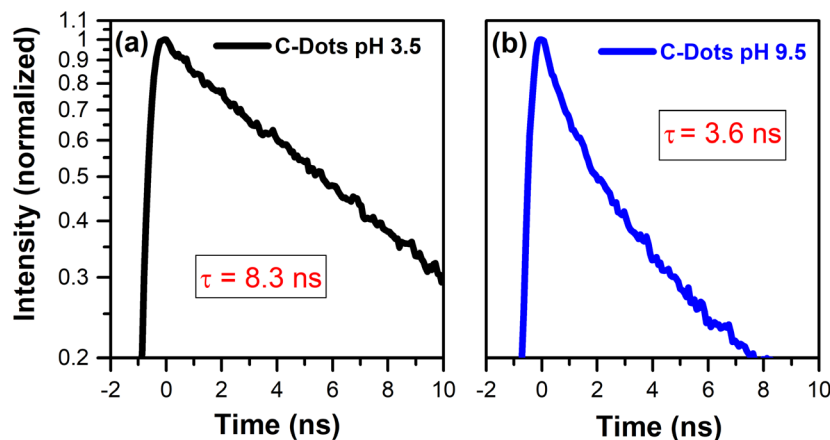


Figure 10. Normalized PL transients of C-Dots dispersed in water with adjusted pH values, excited with 3.54 eV. a) PL transient (black line) of a C-Dots solution with pH 3.5 ± 0.5 ; b) PL transient (blue line) of a C-Dots solution with pH 9.5 ± 0.5 .

(citric acid), the C-Dots are expected to have residual amine and carboxylic groups on their surface.^[49] Citric acid and most aliphatic amines have common acid dissociation constants (pKa) of ≈ 3.1 and $\approx 8-10$, respectively.^[50] Therefore, at pH values close to 3, the carboxylic groups of citric acid are mostly neutral due to the stabilization of negative charges by protons, while amine groups become protonated and positively charged. The positive charge of amine groups results in a reduced probability of the electron transfer between the involved HOMO and LUMO states and therefore in longer decay times.^[51] With increasing pH values up to 9.5 the situation reverses, so that amine groups become neutral and carboxylic groups negatively charged. This finally leads to an increased luminescence transfer rate and the observed reduction in decay time (Figure 10).

Figure 11a shows the photocurrent of bare and functionalized ZnO NWs (hydrothermally grown,^[14] diameter range 50–200 nm, length $\approx 3 \mu\text{m}$) as a function of the photoexcitation energy. The values are calculated as the difference between the current recorded after 20 s of illumination and the background current recorded prior to the measurement.

Pristine ZnO NWs (black dots) show a poor photoresponse under illumination with photon energies below the band gap of ZnO. The slight increase in this range can be attributed to the excitation of defect states in the ZnO.^[25] The photocurrent starts to increase considerably at an excitation energy of about 3.10 eV due to the onset of direct excitation of electrons from the VB to the CB in the ZnO NWs. In contrast, the functionalized devices show a significantly increased photoresponse over the whole studied spectral range except for the NWs functionalized with C-Dots dissolved at pH 1 (pink dots). This is due to the fact, that ZnO NWs may be strongly damaged by the protons during the functionalization with C-Dots at pH 1.

On the other hand, ZnO NWs functionalized with C-Dots at pH 4 (red dots) show an overall enhancement of the photoresponse. The decoration of ZnO NWs with C-Dots at pH 9 (green dots) result in an even stronger photoresponse enhancement at lower photon energies, as compared to NWs treated with C-Dots at pH 4.

To study the impact of the acidic environment on the photoresponse behavior, we performed additional

measurements on ZnO NWs treated only with 0.1 mM HCl (pH 4) as shown in Figure 11b (no C-Dots!). For those NWs, we observed a reduced photoresponse over the whole studied spectral range. This result indicates, that the contribution of the diluted HCl is negligible for the photoresponse enhancement in NWs treated with C-Dots at pH 4.

To explain the enhancement of the photoresponse in functionalized NWs, we propose a model as depicted in Figure 11c. In this model, number (1) describes the absorption and photoexcitation of the electrons in the C-Dots from the HOMO to the LUMO. The enhancement of the photocurrent in functionalized NWs occurs via electron transfer from the LUMO level in the C-Dots to the CB of ZnO NWs (2) as well as other surface processes.^[20,52] The electron injection most probably occurs after the photoexcitation of electron-hole pairs in $n \rightarrow \pi^*$ transitions related to $-\text{C}=\text{O}$ and $-\text{C}-\text{N}-$ groups in the C-Dots.^[49] While the electrons may tunnel from the LUMO of the C-Dots to the CB of the ZnO, the photogenerated holes remain in the HOMO levels of the C-Dots and interact with negatively charged oxygen species at the surface of the ZnO (3). Ionized oxygen species adsorbed at the ZnO NW surfaces lead typically to the formation of surface band bending,^[53] while the desorption of neutral oxygen molecules (4) leads to a reduction of the band bending (5).

The interaction of ionized oxygen species on the ZnO surface with holes left in the C-Dot HOMO results in desorption of the neutral oxygen species, neutralization of the overall charge of the C-Dot surface, and reduction of the surface band bending in the ZnO NWs. Both, the electron transport to the CB of ZnO and the removal of the oxygen species from the ZnO surface contribute to the enhanced photoconductivity due to the increase of the charge carrier density and reduction of the surface band bending, respectively.

6. Structural and Optical Investigation of Hybrid ZnO/Polymer Core-Shell Nanowires Fabricated by oCVD

For the design of many optoelectronic devices based on ZnO and GaN NWs, a conformal coating with a suitable p-conductive material is required.^[5,6,54,55] This material should have a high

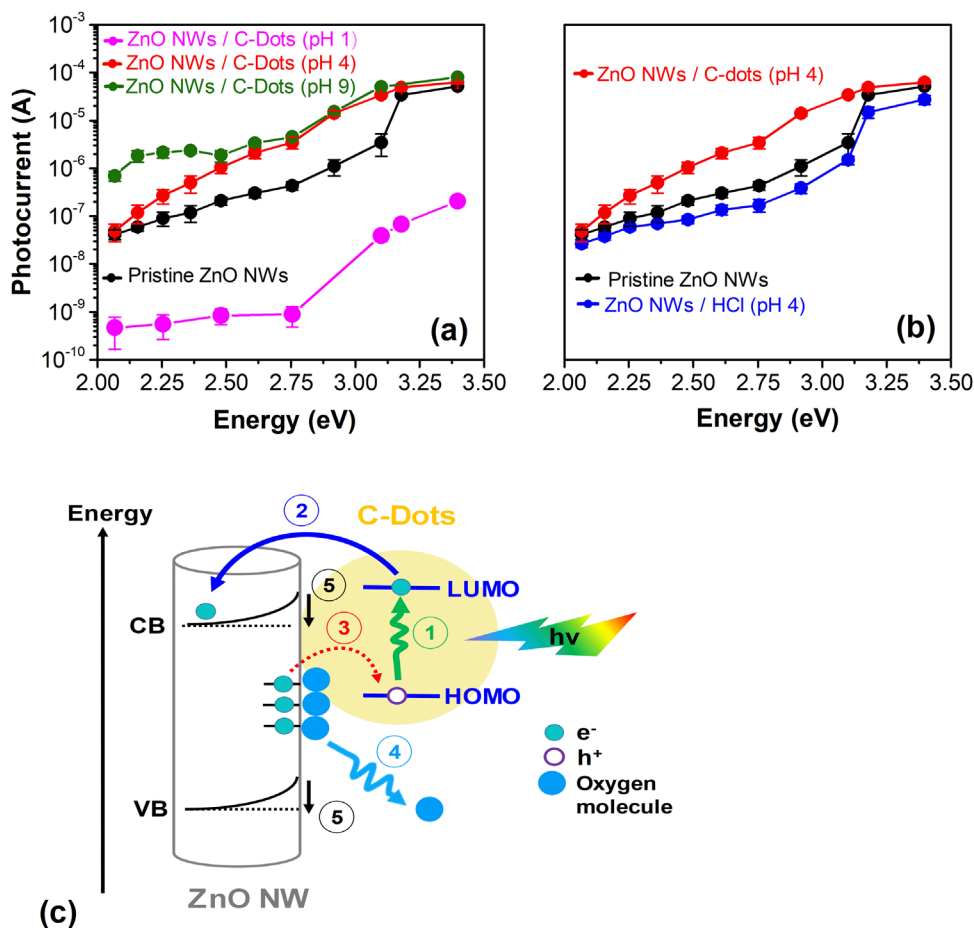


Figure 11. a) Photocurrent of pristine and functionalized ZnO NWs with C-Dots as a function of the excitation energy. The C-Dots were dissolved at different pH-values and deposited on the NWs. b) Comparison of the photoresponse of pristine (black) and functionalized with C-Dots (pH 4, red) ZnO NWs with NWs treated only with 0.1 mM HCl (pH 4, blue) as a function of the excitation energy. c) Physical model explaining the photoconductivity enhancement of ZnO NWs treated with C-Dots (pH 4) under the excitation with photon energies below the band gap of ZnO at ambient conditions (explanation in text). Adapted with permission.^[25] Copyright 2015, American Chemical Society.

lateral conductivity to allow for efficient current spreading and at the same time offer a low series resistance. High transparency in the visible spectral region is required as well as stability under typical operating conditions.^[56] P-type doped ZnO is not available with the outlined specifications,^[57] and even p-type doped GaN still has substantial limitations when it comes to optical quality and high lateral conductivity for efficient current spreading.^[58–60]

The conformal coverage of ZnO- and GaN-based nanowire devices with ultrathin (<100 nm) layers of p-conductive polymers may offer a solution to this limitation. In particular, the oCVD is a powerful and versatile method to achieve such conformal coatings from the gas phase in a completely dry and solventless process.^[57] Yet, the process involved the simultaneous introduction of the gaseous monomer and a suitable oxidant (in many cases FeCl_3) where in particular the oxidant can potentially lead to a deterioration of the surface of the inorganic semiconductor NWs.^[61] As described in the experimental section, we have used the p-conductive polymer PEDOT and PPy for the fabrication and analysis of ZnO-nanowire based hybrid inorganic/organic devices.^[21,26]

Our structural and electrical studies of PPy-coated ZnO layers pointed out that the amount of the oxidizing agent also strongly influences the thickness and homogeneity of the polymer shells.^[26] The use of small amounts of FeCl_3 (0.1 g) leads to smooth interfaces and a good diode-like behavior that will be discussed in section 7.^[21]

In **Figure 12** the results of the structural analysis are depicted. Figure 12a shows an SEM overview image of PPy-coated NWs grown on a silicon substrate (VLS,^[12] length $\approx 3\text{--}5\ \mu\text{m}$, thickness $\approx 150\ \text{nm}$) and a bright-field TSEM image of a single coated NW. Comparable to the case of PPy-coated ZnO layers prepared using 0.1 g FeCl_3 , a thin ($\approx 15\ \text{nm}$) and homogeneous PPy shell is covering the whole nanowire over a large sample area. The EDX measurement (Figure 12b) of the PPy-coated ZnO NWs point to the fact that chlorine is incorporated into the polymer shell as dopant.

The PEDOT shell surrounding the NWs exhibits a completely different behavior. **Figure 13** shows that the polymer is winding around the NWs like filaments resulting in a thin but inhomogeneous coating. A possible reason for this might be the formation of very long polymer chains.

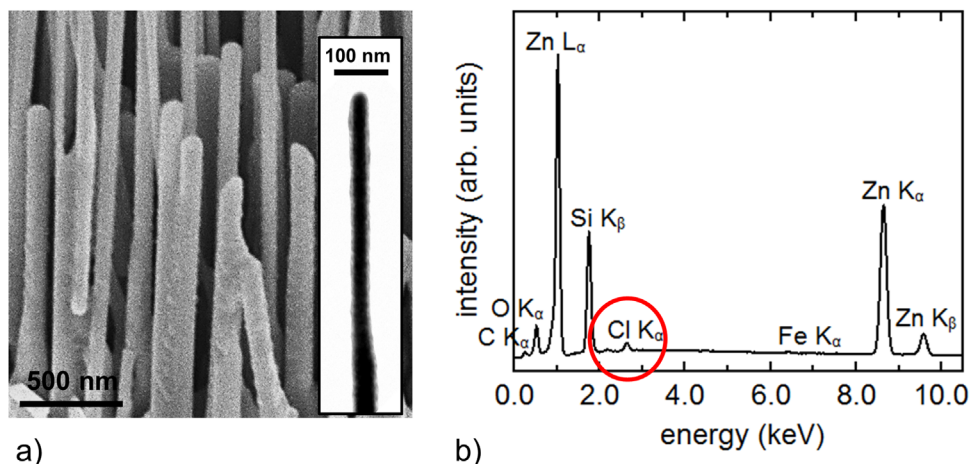


Figure 12. a) SEM overview image of the PPy-coated ZnO NWs. The inset shows a bright-field TSEM image of one single PPy-coated ZnO NW, (b) EDX spectrum of the PPy-coated ZnO NWs showing incorporated Cl. All measurements were performed on the same sample. Adapted with permission.^[26] Copyright 2016, Wiley-VCH.

The PL intensities of the uncoated and the polymer-coated ZnO NWs are depicted in **Figure 14**. The PL spectra are normalized to the near-band-edge (NBE) emission maximum to allow for a comparison of the relative intensities of the deep-level emission (DLE) which is dominant at room temperature. The inset shows the high-resolution PL spectra of the NBE region obtained at $T = 10$ K. The black, red, and blue curves belong to the uncoated, PPy-coated, and PEDOT-coated ZnO NWs, respectively. The DLE gets suppressed for the polymer-coated samples for two possible reasons. On the one hand, the absorption properties of the used polymers^[62,63] may lead to a reduction of the DLE since a considerably reduced photon density reaches the nanowire, on the other hand, the polymer shell may passivate the nanowire surface and thus leads to a decrease of the DLE intensity.

In the high-resolution PL spectrum of the NBE emission of the uncoated wires, the peaks of at least two donor-bound excitons (D^0X), of the surface exciton (SX) and of the first somewhat broadened, in detail unresolved phonon replica

(D^0X-1LO) of the D^0X transitions can be clearly identified. A band at 3.32 eV indicates a defect-related emission. In case of the PPy-coated NWs (red curve), the SX peak is suppressed most probably through passivation of the NW surface states by the polymer shell. However, the D^0X peaks and the phonon replica are still clearly visible. In the energy region above 3.36 eV a slight broadening of the lines appears which is probably caused by the absorption of PPy. In contrast to that, the PEDOT-coated sample shows a broadening of the entire NBE emission. Previous studies have revealed that the aggressive oxidizing agent (either incorporated bromine or, as in our case, chlorine) induces an augmentation of structural

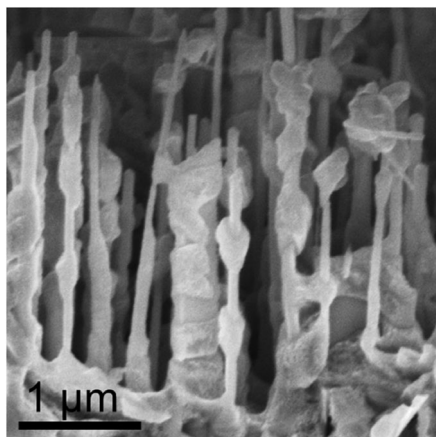


Figure 13. SEM overview image of PEDOT-coated ZnO NWs. Adapted with permission.^[26] Copyright 2016, Wiley-VCH.

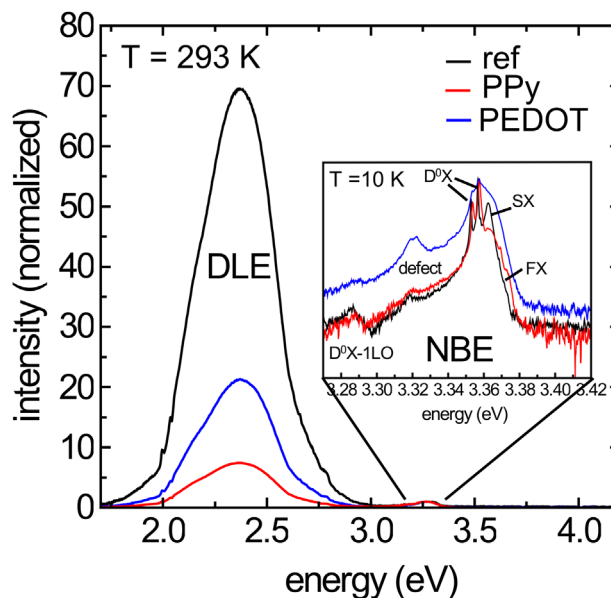


Figure 14. Normalized overview PL spectra taken at room temperature for the uncoated (black), PPy- (red), and PEDOT- (blue) coated ZnO NWs. The inset is showing the high resolution PL spectra of the NBE taken at $T = 10$ K. Adapted with permission.^[26] Copyright 2016, Wiley-VCH.

defects on the nanowire surface which leads to the formation of centers with various localization energies.^[64] Nevertheless, from the overview and high-resolution PL spectra it becomes visible that the overall optical properties of the ZnO NWs are not significantly affected by the different polymer coatings as far as energy position and spectral width of the emission bands is concerned. The UV emission peak is broadened but the defect luminescence seemed nearly unaffected except for the different intensity ratios. Obviously, it is possible to achieve a thin and conformal polymer coating in the nanometer range via the oCVD method without causing strong deformation of the NW surfaces.

7. Electrical Characterization of Hybrid Inorganic/Organic Layered Interfaces

Electrical studies on planar PPy/pc-ZnO (polycrystalline ZnO) structures identified a diode like behavior that is strongly impacted by the use of different FeCl₃ amounts during the oCVD polymer growth process.^[20,21] Figure 15 shows the current–voltage (*I*–*V*) characteristics of planar PPy/pc-ZnO for three different amounts of the oxidizing agent during the growth process.

The experimental *I*–*V* curves were modeled by an equivalent circuit to analyze the impact of the oxidizing agent on the diodes' behavior. The model applied is depicted in the inset of Figure 15. The circuit is described as a diode with a parallel resistance (*R_p*) related to leakage currents. These contributions describe the junction interface. Bulk effects are described with the series resistance of the system (*R_s*) in parallel to a space charge limited current (SCLC).^[21] A fundamental parameter of the diode is the ideality factor η . An ideal diode with diffusion or thermionic emission as the conduction mechanism is described with an

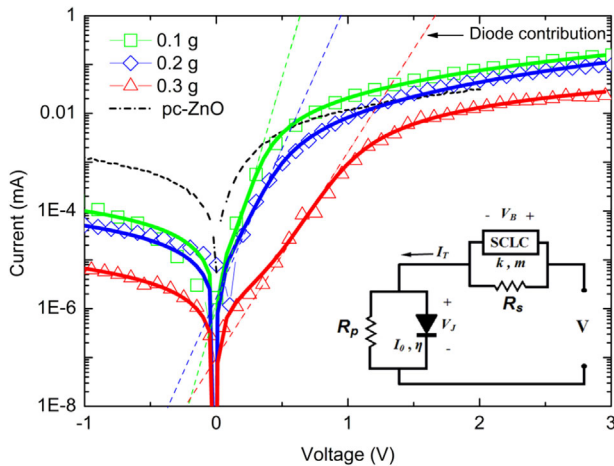


Figure 15. Current–voltage characteristics (symbols) and modeling (solid lines) of planar PPy/pc-ZnO structures and the uncoated pc-ZnO surface (black dash-dotted). The PPy-layer was grown via oCVD with different amounts of the oxidizing agent FeCl₃. Using a correlated circuit diode model (inset), the *I*–*V* characteristics could be traced back and the diode contribution (dashed lines) was identified. Adapted with permission.^[21] Copyright 2016, John Wiley & Sons.

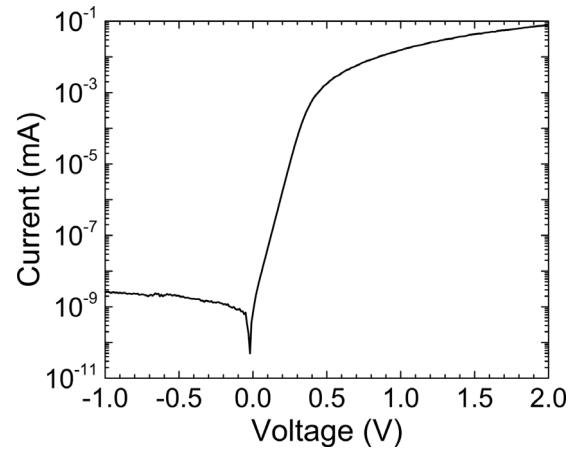


Figure 16. Current–voltage characteristic of a PEDOT/ZnO layered structure. The PEDOT layer was grown by oCVD and has a thickness of about 40 nm.

ideality factor $\eta = 1$; $1 < \eta < 2$ indicates recombination and higher ideality factors of $\eta > 2$ are observed for tunneling through trap states.^[65] Applying the general diode equation $I_D = I_0 [\exp(qV_j / \eta k_B T) - 1]$ with the diode current I_D , saturation current I_0 , junction voltage V_j , Boltzmann constant k_B , and temperature T , yields ideality factors of 1.7 and 4 for 0.1 and 0.3 g, respectively.^[21] This highlights a stronger defect formation at the interface for higher amounts of the oxidizing agent used for the deposition process of the polymer.

Similarly, the general diode equation was used to model the linear slope in forward bias to identify the diode contribution of PEDOT/ZnO junctions. The hybrid interface of a PEDOT/ZnO-layered structure, where the PEDOT film with a thickness of 40 nm was grown by oCVD on PLD-grown about 600 nm thick ZnO, shows a strong rectification with a ratio of about 10^7 at ± 1 V (see Figure 16). This rectification ratio outperforms the previously discussed PPy/ZnO rectification ratio by five orders of magnitude. However, it has to be taken into account, that the pc-ZnO film thickness is much thinner (roughly factor of 10) in this case. Ideality factor values for PEDOT/ZnO-layered structures as shown in Figure 16 range from 1.1 to 1.3. PEDOT/ZnO hybrid junctions show pronounced diode-like behavior and are therefore promising for further research in the field of hybrid optoelectronic devices.

8. Conclusion

In conclusion, we have studied the optical properties and carrier dynamics in inorganic and hybrid inorganic/organic semiconductor nanowire structures based on the ZnO and GaN material systems. We have analyzed the recombination dynamics in 3D GaN-based microrod LED structures at excitation densities close to the damage threshold and found a change in the intensity ratio of the maximum GaN PL intensity relative to that of the InGaN PL which becomes irreversible for excitation energy density $> 0.05 \text{ J cm}^{-2}$. The decay dynamics of the 3D structures are not influenced by the QCSE due to the growth of the InGaN QWs on the non-polar sidewalls. We studied the recombination dynamics

depending on the temperature and the excitation photon energy and found just a small influence of thermal activated defect states and of electrons refilling the InGaN states by relaxation out of the GaN. An increase of the excitation density by about two orders of magnitude leads to a decrease of the decay time by about 30% due to band filling effects.

We have furthermore studied the carrier dynamics in nanowire structures functionalized with colloidal CdSe QDs or carbon nanoparticles (C-Dots). In photoconductivity experiments, light absorption in the CdSe QDs at photon energies below the band gap of the ZnO NWs still results in an increased photoconductivity of the NWs. The dynamics of this change of the photoconductivity are dominated by the oxygen de- and adsorption processes at the nanowire and QDs surfaces. From time-resolved PL measurements, we have determined the tunneling rate of photo-excited electrons from the QDs to the NWs to be about 200 MHz (corresponding to a time constant of 5 ns). Furthermore, we have studied the dependence of the tunneling rate on the length of the organic linker molecules that are used to attach the QDs to the nanowire surface and found higher rates for shorter linker molecules. We have also shown that carbon nanoparticles (C-Dots) present an interesting alternative to CdSe QDs because they show similar properties as photo-sensitizer when applied to ZnO nanowire devices.

Finally, we demonstrated the fabrication of nanowire/polymer core-shell structures by oCVD. We showed that the oCVD process can be optimized such that the electronic transport across the hybrid interface (i.e., between the p-conductive polymer shell and the n-conductive nanowire core) is dominated by thermionic emission. This can be inferred from the ideality factors of the optimized hybrid diodes that were in the range $1 < \eta < 2$. Deposition of PEDOT layers on planar ZnO substrates by the oCVD process resulted in hybrid devices with rectification ratios as high as 10^7 at ± 1 V. This demonstrates the huge potential of oCVD for the fabrication of high-quality hybrid inorganic/organic nanowire-based radial pn-junctions with applications as optoelectronic or sensing devices.

Acknowledgements

The authors thank the groups of Andreas Waag, TU Braunschweig, Margit Zacharias, University of Freiburg, Carsten Ronning, University of Jena, Marius Grundmann, University of Leipzig, and Siegfried R. Waldvogel, University of Mainz, for providing the samples. Further, we thank Zhipeng Zhang, Daniel Splith, Holger Hochmuth, Holger von Wenckstern, and Marius Grundmann (University of Leipzig) for the experimental support and discussions concerning the electrical characterization of hybrid PEDOT/ZnO structures and Karen Gleason and Xiaoxue Wang (Massachusetts Institute of Technology) for the insights into oCVD. We further thank the group of Lutz Mädler (IWT, University of Bremen) for collaboration and use of their oCVD equipment. We gratefully acknowledge funding by the DFG research unit FOR 1616 "Dynamics and Interactions of Semiconductor Nanowires for Optoelectronics," by the combined University of Bremen/FP7-PEOPLE-2012 COFUND Marie-Curie Fellowship "Bremen Trac," project no. 600411, by "Niedersächsisches Vorab" through "Quantum- and Nano-Metrology (QUANO-MET)" initiative within the project NL-3 "Sensors" and NP-3 "Modell-Nanopartikel," by the DFG Research Training Group GrK1952/1 "Metrology for Complex Nanosystems" and the Braunschweig International Graduate School of Metrology B-IGSM.

Conflict of Interest

The authors declare no conflict of interest.

Keywords

colloidal quantum dots, hybrid nanostructures, organic polymers, oxidative chemical vapor deposition, time-resolved photoluminescence

Received: September 5, 2018

Revised: December 20, 2018

Published online: February 20, 2019

- [1] G. Suo, S. Jiang, J. Zhang, J. Li, M. He, *Adv. Condens. Matter Phys.* **2014**, 2014, 456163.
- [2] Ü. Özgür, D. Hofstetter, H. Morkoç, *Proc. IEEE* **2010**, 98, 1255.
- [3] A. Waag, X. Wang, S. Fündling, J. Ledig, M. Erenburg, R. Neumann, M. Al Suleiman, S. Merzsch, J. Wei, S. Li, H. H. Wehmann, W. Bergbauer, M. Strassburg, A. Trampert, U. Jahn, H. Riechert, *Phys. Status Solidi C* **2011**, 8, 2296.
- [4] M. Mandl, X. Wang, T. Schimpke, C. Kölper, M. Binder, J. Ledig, A. Waag, X. Kong, A. Trampert, F. Bertram, J. Christen, F. Barbagini, E. Calleja, M. Strassburg, *Phys. Status Solidi RRL – Rapid Res. Lett.* **2013**, 7, 800.
- [5] T. Voss, S. R. Waldvogel, *Mater. Sci. Semicond. Process.* **2017**, 69, 52.
- [6] F. Meierhofer, L. Krieg, T. Voss, *Semicond. Sci. Technol.* **2018**, 33, 083001.
- [7] C. W. Bunn, *Proc. Phys. Soc.* **1935**, 47, 835.
- [8] C. A. Mead, *Phys. Lett.* **1965**, 18, 218.
- [9] S. J. Xu, W. Liu, M. F. Li, *Appl. Phys. Lett.* **2002**, 81, 2959.
- [10] K. A. Bertness, N. A. Sanford, A. V. Davydov, *IEEE J. Sel. Top. Quantum Electron.* **2011**, 17, 847.
- [11] X. Wang, S. Li, M. S. Mohajerani, J. Ledig, H. H. Wehmann, M. Mandl, M. Strassburg, U. Steegmüller, U. Jahn, J. Lähnemann, H. Riechert, I. Griffiths, D. Cherns, A. Waag, *Cryst. Growth Des.* **2013**, 13, 3475.
- [12] H. Choi, in *Semiconductor Nanostructures for Optoelectronic Devices: Processing, Characterization and Applications* (Ed: G.-C. Yi), Springer-Verlag, Berlin, Heidelberg **2012**, pp. 1–36.
- [13] T. Ma, M. Guo, M. Zhang, Y. Zhang, X. Wang, *Nanotechnology* **2007**, 18, 035605.
- [14] G. Hua, Y. Tian, L. Yin, L. Zhang, *Cryst. Growth Des.* **2009**, 9, 4653.
- [15] K. Subannajui, A. Menzel, F. Güder, Y. Yang, K. Schumann, X. Lu, M. Zacharias, *Adv. Funct. Mater.* **2013**, 23, 191.
- [16] J. Hartmann, MOVPE selective area growth of GaN/InGaN rod and fin core-shell LEDs, *PhD Dissertation*, University of Technology Braunschweig, **2018**.
- [17] X. Chen, J. L. Hutchison, P. J. Dobson, G. Wakefield, *J. Mater. Sci.* **2009**, 44, 285.
- [18] V. V. Breus, C. D. Heyes, G. U. Nienhaus, *J. Phys. Chem. C* **2007**, 111, 18589.
- [19] S. Hu, A. Trinchì, P. Atkin, I. Cole, *Angew. Chemie – Int. Ed.* **2015**, 54, 2970.
- [20] S. Bley, M. Diez, F. Albrecht, S. Resch, S. R. Waldvogel, A. Menzel, M. Zacharias, J. Gutowski, T. Voss, *J. Phys. Chem. C* **2015**, 119, 15627.
- [21] A. Castro-Carranza, J. C. Nolasco, S. Bley, M. Rückmann, F. Meierhofer, L. Mädler, T. Voss, J. Gutowski, *J. Polym. Sci. B, Polym. Phys.* **2016**, 54, 1537.
- [22] A. Vogt, J. Hartmann, H. Zhou, M. S. Mohajerani, S. Fündling, B. Szafranski, H. H. Wehmann, A. Waag, T. Voss, T. Schimpke, A. Avramescu, M. Strassburg, *J. Mater. Res.* **2017**, 32, 2456.
- [23] A. Jaros, J. Hartmann, H. Zhou, B. Szafranski, M. Strassburg, A. Avramescu, A. Waag, T. Voss, *Sci. Rep.* **2018**, 8, 11560.

- [24] S. Bley, F. Albrecht, S. Resch, S. R. Waldvogel, A. Menzel, M. Zacharias, T. Voss, J. Gutowski, *Phys. Status Solidi C* **2016**, *13*, 606.
- [25] D. Cammi, K. Zimmermann, R. Gorny, A. Vogt, F. Dissinger, A. Gad, N. Markiewicz, A. Waag, J. D. Prades, C. Ronning, S. R. Waldvogel, T. Voss, *J. Phys. Chem. C* **2018**, *122*, 1852.
- [26] S. Bley, M. Rückmann, A. Castro-Carranza, F. Meierhofer, L. Mädler, T. Voss, J. Gutowski, *Phys. Status Solidi C* **2016**, *13*, 614.
- [27] Y. J. Hong, C. H. Lee, A. Yoon, M. Kim, H. K. Seong, H. J. Chung, C. Sone, Y. J. Park, G. C. Yi, *Adv. Mater.* **2011**, *23*, 3284.
- [28] B. O. Jung, S. Bae, S. Lee, S. Y. Kim, J. Y. Lee, Y. Honda, H. Amano, *Nanoscale Res. Lett.* **2016**, *11*, 215.
- [29] P. Waltereit, O. Brandt, A. Trampert, H. T. Grahn, J. Menniger, M. Ramsteiner, M. Reiche, K. H. Ploog, *Nature* **2000**, *406*, 865.
- [30] T. Langer, M. Klisch, F. Alexej Ketzler, H. Jönen, H. Bremers, U. Rossow, T. Meisch, F. Scholz, A. Hangleiter, *Phys. Status Solidi B* **2016**, *253*, 133.
- [31] J. S. Im, H. Kollmer, J. Off, A. Sohmer, F. Scholz, A. Hangleiter, J. Seo Im, H. Kollmer, J. Off, A. Sohmer, F. Scholz, A. Hangleiter, *Phys. Rev. B* **1998**, *57*, R9435.
- [32] T. Takeuchi, S. Sota, M. Katsuragawa, M. Komori, H. Takeuchi, H. Amano, I. Akasaki, *Jpn. J. Appl. Phys.* **1997**, *36*, L382.
- [33] J. Feldmann, G. Peter, E. O. Göbel, P. Dawson, K. Moore, C. Foxon, R. J. Elliott, *Phys. Rev. Lett.* **1987**, *59*, 2337.
- [34] L. C. Andreani, F. Tassone, F. Bassani, *Solid State Commun.* **1991**, *77*, 641.
- [35] P. Lefebvre, J. Allègre, B. Gil, A. Kavokine, H. Mathieu, W. Kim, A. Salvador, A. Botchkarev, H. Morkoç, *Phys. Rev. B* **1998**, *57*, R9447.
- [36] D. Rosales, T. Bretagnon, B. Gil, A. Kahouli, J. Brault, B. Damilano, J. Massies, M. V. Durnev, A. V. Kavokin, *Phys. Rev. B* **2013**, *88*, 125437.
- [37] S. Marcinkevičius, K. M. Kelchner, L. Y. Kuritzky, S. Nakamura, S. P. Denbaars, J. S. Speck, *Appl. Phys. Lett.* **2013**, *103*, 111107.
- [38] K. Köhler, R. Gutt, J. Wiegert, L. Kirste, *J. Appl. Phys.* **2013**, *113*, 073514.
- [39] C. Lee, S. Kim, K. Lim, *J. Korean Phys. Soc.* **1999**, *35*, 280.
- [40] E. S. Jeon, V. Kozlov, Y. K. Song, A. Vertikov, M. Kuball, A. V. Nurmikko, H. Liu, C. Chen, R. S. Kern, C. P. Kuo, M. G. Craford, *Appl. Phys. Lett.* **1996**, *69*, 4194.
- [41] H. Wang, E. R. McNellis, S. Kinge, M. Bonn, E. Cánovas, *Nano Lett.* **2013**, *13*, 5311.
- [42] K. S. Leschkes, R. Divakar, J. Basu, E. Enache-Pommer, J. E. Boercker, C. B. Carter, U. R. Kortshagen, D. J. Norris, E. S. Aydil, *Nano Lett.* **2007**, *7*, 1793.
- [43] R. Gurwitz, R. Cohen, I. Shalish, *J. Appl. Phys.* **2014**, *115*, 033701.
- [44] D. Hou, A. Dev, K. Frank, A. Rosenauer, T. Voss, *J. Phys. Chem. C* **2012**, *116*, 19604.
- [45] S. Y. Lim, W. Shen, Z. Gao, *Chem. Soc. Rev.* **2015**, *44*, 362.
- [46] X. Li, M. Rui, J. Song, Z. Shen, H. Zeng, *Adv. Funct. Mater.* **2015**, *25*, 4929.
- [47] H. Li, Z. Kang, Y. Liu, S. T. Lee, *J. Mater. Chem.* **2012**, *22*, 24230.
- [48] Y. P. Sun, B. Zhou, Y. Lin, W. Wang, K. A. S. Fernando, P. Pathak, M. J. Mezziani, B. A. Harruff, X. Wang, H. Wang, P. G. Luo, H. Yang, M. E. Kose, B. Chen, L. M. Veca, S. Y. Xie, *J. Am. Chem. Soc.* **2006**, *128*, 7756.
- [49] J. Schneider, C. J. Reckmeier, Y. Xiong, M. Von Seckendorff, A. S. Susha, P. Kasak, A. L. Rogach, *J. Phys. Chem. C* **2017**, *121*, 2014.
- [50] D. R. Lide, *CRC Handbook of Chemistry and Physics*. CRC Press, Boca Raton, FL **2003**.
- [51] S. Draxler, M. E. Lippitsch, *Sens. Actuators B, Chem.* **1995**, *29*, 199.
- [52] B. J. Yang, J. T. Chen, L. F. Cui, W. W. Liu, *RSC Adv.* **2015**, *5*, 59204.
- [53] D. A. Melnick, *J. Chem. Phys.* **1957**, *26*, 1136.
- [54] Z. Wang, P. Xiao, L. Qiao, X. Meng, Y. Zhang, X. Li, F. Yang, *Physica B – Condens. Matter* **2013**, *419*, 51.
- [55] M. Willander, O. Nur, S. Zaman, A. Zainelabdin, N. Bano, I. Hussain, *J. Phys. D: Appl. Phys.* **2011**, *44*, 224017.
- [56] W. Lövenich, *Polym. Sci. C* **2014**, *56*, 135.
- [57] J. P. Lock, S. G. Im, K. K. Gleason, *Macromolecules* **2006**, *39*, 5326.
- [58] G. Li, W. Wang, W. Yang, Y. Lin, H. Wang, Z. Lin, S. Zhou, *Rep. Prog. Phys.* **2016**, *79*, 056501.
- [59] S. Nakamura, T. Mukai, M. Senoh, N. Iwasa, *Jpn. J. Appl. Phys.* **1992**, *31*, L139.
- [60] T. Tanaka, A. Watanabe, H. Amano, Y. Kobayashi, I. Akasaki, S. Yamazaki, M. Koike, *Appl. Phys. Lett.* **1994**, *65*, 593.
- [61] W. E. Tenhaeff, K. K. Gleason, *Adv. Funct. Mater.* **2008**, *18*, 979.
- [62] S. G. Im, K. K. Gleason, *Macromolecules* **2007**, *40*, 6552.
- [63] J. L. Brédas, J. C. Scott, K. Yakushi, G. B. Street, *Phys. Rev. B* **1984**, *30*, 1023.
- [64] J. P. Richters, A. Dev, C. Ronning, J. Gutowski, T. Voss, *J. Phys. D: Appl. Phys.* **2014**, *47*, 394004.
- [65] A. G. Milnes, D. L. Feucht, *Heterojunctions and Metal-Semiconductor Junctions*. Academic Press, New York **1972**.